Synthesis of palladium phosphides for aqueous phase hydrodechlorination: Kinetic study and deactivation resistance

Zhijie Wu, [a]* Tao Pan, [a] Yan Chai, [b] Shaohui Ge, [c] Yana Ju, [c] Tianshu Li, [c] Kai Liu, [c] Ling Lan, [c] Alex C. K. Yip, [d]* Minghui Zhang [b]*

[a] State Key Laboratory of Heavy Oil Processing and the Key Laboratory of Catalysis of CNPC, China University of Petroleum, Beijing, 102249, China

[b] Key Laboratory of Advanced Energy Materials Chemistry (Ministry of Education), College of Chemistry, Nankai University, Tianjin 300071, China

[c] Petrochemical Research Institute, PetroChina Company Limited, E318, A42 Block, China Petroleum Innovation Base, Changping, Beijing, 100195, China

[d] Department of Chemical and Process Engineering, University of Canterbury, Christchurch, New Zealand

*Corresponding author.

Zhijie Wu

Tel.: +86 10 8973 3235;

Fax: +86 10 8973 4979.

E-mail address: zhijiewu@cup.edu.cn (Z.J. Wu)

Alex C. K. Yip

E-mail address: alex.yip@canterbury.ac.nz

Minghui Zhang

E-mail address: zhangmh@nankai.edu.cn

Abstract

We report the synthesis of noble metal phosphides by a temperature-programmed reduction method for aqueous hydrodechlorination (HDC) of 4-chlorophenol (4-CP). $Pd_3P_{0.95}/SiO_2$, Rh_2P/SiO_2 and PtP_2/SiO_2 catalysts were prepared and showed higher 4-CP HDC rates than their corresponding noble metal catalysts. $Pd_3P_{0.95}/SiO_2$ sample exhibited a higher HDC rate than the other phosphide catalysts and Pd/SiO_2 catalysts. The XPS spectra show the surface interaction reactions of the Pd and P species that occur via the electron transfer from Pd to P. $Pd_3P_{0.95}/SiO_2$ was synthesized with different phosphide particle size (1.1~13.5 nm) via changing the metal loading from 1 to 10 wt. %. The 4-CP HDC reaction is sensitive to the size of the Pd and $Pd_3P_{0.95}$ particles, and the optimum sizes for Pd/SiO_2 and $Pd_3P_{0.95}/SiO_2$ were ~8 and ~5 nm, respectively. The effects of the initial 4-CP and Cl ion concentration and the S to Pd_{surf} (surface active Pd metal sites determined by hydrogen chemisorptions) ratio on the 4-CP HDC activity were examined for both catalysts. The Langmuir-Hinshelwood kinetic model that was developed considering the surface reaction as the rate-determining step suggests P has an enhancing effect on sorption in the 4-CP reaction and an inhibiting effect on chloride sorption for $Pd_3P_{0.95}/SiO_2$. Moreover, $Pd_3P_{0.95}/SiO_2$ possesses better sulfide resistance than Pd/SiO_2 because P can prevent the conversion of Pd metallic sites into inactive Pd_4S compounds with a sulfide treatment. As a result, $Pd_3P_{0.95}/SiO_2$ shows better HDC stability than those of Pd/SiO_2 catalysts.

Key words: Hydrodechlorination; metal phosphide; 4-chlorophenol; noble metal;

catalyst.

1. Introduction

The removal of organochlorinated pollutants is a pressing problem in water treatment due to their toxicity and tightened environmental policies [1, 2]. Among all chlorinated organic compounds, chlorophenols (CPs, typically 50~500 mg L^{-1} in wastewater that contains phenols) require effective remediation due to their high toxicity, persistency, low biodegradability [3, 5]and their present in both surface and ground water. Catalytic hydrodechlorination (HDC) reaction has been investigated in the past decade and is found to be very effective in eliminating aqueous chlorinated pollutants, such as chlorophenols, using hydrogen over a wide range of concentrations at ambient or near-ambient temperatures [6, 7]. Because of the low solubility of CPs in water, kinetic analysis of HDC in aqueous solution has been mainly limited to 4-CP (4-chlorophenol) since it is relatively soluble (ca. 27 g L^{-1} (0.21 mol L^{-1}) in water at 293 K) compared with its isomers [5， 7-10]. In order to develop a more effective catalyst and to build a kinetic database for industrial process, it is important to advance the fundamental understanding of catalytic HDC of chlorophenols.

Beside Raney Ni [11] catalysts, noble metal catalysts, especially Pd [12-25], Pt [6, 26] and Rh [27-29] metal catalysts and Pd-based bimetallic catalysts [30-33], have been reported to be good catalysts for the aqueous-phase CP HDC reaction under mild conditions. For example, Yuan et al.[14] and Roy et al. [16] achieved the HDC of CPs over Pd-based catalysts at ambient temperatures (273-303 K) under atmospheric

pressure. The main products from the HDC reaction of monochlorophenol over Pd-based catalysts are typically phenol (e.g., >90% selectivity), cyclohexanone, and trace amount of cyclohexanol (<0.05% selectivity) [14, 34]. The most commonly used support materials are alumina and activated carbon (AC) [14, 16]. While the turnover frequency (TOF) of HDC of 4-CP over Pd/C catalyst ranging from 0.12 to 0.17 $mol_{4\text{-}CP}$ $mol_{active\text{-}Pd}^{-1}$ s^{-1} [19, 35-37], it can be further increased to between 0.43 and 0.7 $mol_{4\text{-}CP}$ $mol_{active\text{-}Pd}^{-1}$ s^{-1} by modifying the carbon support itself or introducing polymers to the catalyst matrix.

Factors that influence activity and selectivity, such as the relationships between the size of the metallic phase clusters and the HDC performance, have been studied [20, 38]. The HDC of 4-chlorophenol is a structural sensitive reaction [39] that the activity-and-size correlation revealed a volcano plot with Rh metal clusters being the optimum. Among all tested metals, Pd is the least susceptible to catalytic poisoning due to chloride ions. Itis also considered as the most suitable active phase catalyst for the liquid phase HDC reactions [7, 12-25, 40], especially for the system in which carbon materials are used as the support. The carbon supported catalysts exhibited high HDC activities due to promotion of reactive spillover hydrogen [9] or enhancement of the sorption of CPs [41]. A critical issue associated with the liquid phase HDC is that substantial catalyst deactivation can easily happen due to metal leaching caused by the HCl by-product. Nevertheless, due to the weak acidity of CPs, the addition of base can help increase the solubility and limit the HCl poisoning [8]. In the study, a kinetic analysis based on the Langmuir–Hinshelwood mechanisms is performed. The effect of the size

of the active phase on the HDC and the applicability of the kinetic model are carefully assessed.

The rise of sulfur utilization in various chemical industries in the last decade not only means that the sulfur present in water and wastewater is becoming more significant, but the form of sulfur also varies from HS^-, S^{2-}, SO_4^{2-}, SO_3^{2-} and to other sulfur-containing anions. On the other hand, the widespread water contamination with chlorinated solvents, pesticides and sulfur has spurred intense effort to develop efficient and cost-effective treatment methods for chlorinated compounds, especially with co-contamination of sulfur. The HDC reactions over metal catalysts are regarded as a potential route to remove chlorinated compounds. However, the metal catalysts are often suffered from deactivation due to chloride (Cl^-) and hydrosulfide (SH^- or "sulfide" in short) ions [30, 42, 43]. Therefore, the strong poisoning effects associated with traces of sulfur compounds need to be addressed in order to develop noble metal catalysts with long-term durability. For example, Wong et al. developed Pd/Au nanoparticles for HDC reaction of trichloroethene in aqueous phase by promoting the effect of gold on the catalyst resistance to sulfur poisoning at room temperature [30].

In light of the excellent performance of metal phosphides in hydrotreating reactions, such as hydrodesulfurization (HDS) [44-50], metal phosphides should be suitable catalysts for the HDC reaction and have a sulfur resistance. In the past 10 years, transition-metal phosphides have been used in the gas-phase HDC reaction at high temperatures because their activities are lower than those of noble metal catalysts at

low reaction temperature [51-53]. Little work has been devoted to the catalytic performance of noble metal phosphide catalysts in the aqueous-phase HDC reaction. Here, we firstly screened noble metal phosphides (platinum, rhodium and palladium phosphides) for the aqueous-phase HDC reaction of 4-chlorophenol (4-CP). We studied the effects of sulfide and chloride ions on the 4-CP HDC reaction rates of the palladium phosphide catalyst and observed that chloride and sulfide had slight effects that were markedly less than those observed with the Pd catalyst. To clarify the chloride and sulfide resistances of the noble metal phosphide in the aqueous HDC reaction, reaction kinetic models based on the Langmuir-Hinshelwood (L-H) model have been extensively applied to investigate the catalytic process.

2. Experimental section

2.1. Chemicals

$NH_4H_2PO_4$ (≥99%), $NH_3•H_2O$ (25~28%), NaCl (≥99.5%), NaOH (≥96%) and Na_2S (≥98.0%) were purchased from Guanfu Chemical, Ltd. (Tianjin, China). $PdCl_2$ (60% Pd basis), H_2PtCl_6 (≥99.8%), $RhCl_3•xH_2O$ (39% Rh), 4-chlorophenol (≥99%), $AgNO_3$ (99.8%), phenol (≥99%), cyclohexanone (≥99.5%) and cyclohexanol (≥98%) were obtained from Sinopharm Chemical Reagent Co., Ltd. (Beijing). All the reagents were used as purchased without any further purification.

Silica gel (SiO_2, 99%) was obtained from the China National Offshore Oil Corp. (CNOOC) Tianjin Chemical Research and Design Institute (Tianjin, China). For the catalyst preparation, SiO_2 was dried at 393 K in an oven for 6 h and then calcined in air

at 823 K for 4 h.

2.2. Catalyst synthesis

The SiO_2-supported noble metal phosphides (PtP_2, $Pd_3P_{0.95}$, and Rh_2P) were successfully prepared by a temperature-programmed reduction (TPR) method [45]. Ammonium dihydrogen phosphate ($NH_4H_2PO_4$) was used as the phosphorus source. $PdCl_2$ and $RhCl_3 \cdot xH_2O$ were dissolved in an ammonia solution to create a homogenous clear solution. A typical TPR method procedure is described as follows. First, $PdCl_2$, $RhCl_3 \cdot xH_2O$ and H_2PtCl_6 solutions with various concentrations were prepared to obtain supported catalysts with 1, 2, 3, 5 and 10 wt.% noble metal loadings. Then, the noble metal salt solution was mixed with the $NH_4H_2PO_4$ solution. To obtain pure phase of phosphide, various ratios of P to noble metal in raw materials were screened and an atomic ratio of P to noble metal of 2 (for Pd), 5 (for Pt) and 4/3 (for Rh) has been achieved. SiO_2 was then added to the solutions with at a solid to solution weight ratio of 1/20, and the mixture was stirred (400 rpm) for 4 h and subsequently treated at 318 K overnight under rotation in a rotary evaporator to remove the water. The solid samples were treated in ambient air at 373 K for 6 h and then heated in air at 673 K (0.067 K s^{-1}) for 3 h. To obtain the phosphides, the calcined samples were treated in pure hydrogen gas (1 cm^3 g^{-1} s^{-1}) from room temperature to 523 K (0.067 K s^{-1}), and then, they were treated in pure hydrogen gas (1 cm^3 g^{-1} s^{-1}) at 773 K (0.033 K S^{-1}) for 5 h. The samples were passivated under 0.5% O_2/Ar (0.5 cm^3 g^{-1} s^{-1}) for 1 h at 300 K before air exposure.

The SiO_2-supported noble metal catalysts were prepared with procedures similar to those of the metal phosphides without the introduction of $NH_4H_2PO_4$. To obtain the

metallic sites, the samples were directly reduced in pure hydrogen gas (1 cm^3 g^{-1} s^{-1}) at 673 K (0.033 K S^{-1}) for 4 h. The samples were passivated under 0.5 vol. % O_2/Ar (0.5 cm^3 g^{-1} s^{-1}) for 1 h at 300 K before air exposure.

To obtain supported noble metal catalyst samples with different metal particle sizes, the precursors of the metal catalysts were treated in flowing dry air (1.0 cm^3 g^{-1} s^{-1}) by increasing the temperature to 673–873 K at 0.05 K s^{-1} and holding the samples there 5 h to prepare samples with a broad range of metal fraction dispersion (0.07–0.97, Table 1 for Pd/SiO_2 samples with 5 wt.% theory metal loading) measured by H_2 chemisorptions as described below.

2.3. Catalyst characterization

The powder X-ray diffraction (XRD) patterns of the obtained samples were collected on a Bruke AXS D8 Advance X-ray diffractometer with Cu Kα radiation (λ=1.5406 Å, 40 kV, 40 mA) at a scanning rate of 4° /min in the range of 10-80° (2θ). The size and morphology of the as-synthesized samples were observed on a Tecnai G2 F20 transmission electron microscope (TEM) operated at 200 kV. The TEM specimens were prepared by dispersing the samples in ethanol by ultrasonication for 3 min and depositing the dispersed samples onto on carbon-coated Cu grid. Metal cluster size distributions were determined by counting > 400 crystallites. The surface area-weighted cluster diameters, d_{TEM}, were calculated using $d_{TEM} = \sum n_i d^3 / n_i d^2$ [54].

The metal loading of the samples was determined by X-ray fluorescence (XRF) conducted on a PANalytical AxiosMAX analyser. X-ray photoelectron spectroscopy

(XPS) with a Fluorolog-Tau-3 (ISA-USA) was used to examine the electronic properties of the catalysts with non-monochromatized Mg Kα radiation as the excitation source, and the binding energies were calibrated using a C 1s binding energy of 284.8 eV. The surface of the fresh samples was etched with Ar^+ ions for 15 min to remove the oxided layer. The peaks were fitted by a nonlinear least square fitting program using a properly weighted sum of the Lorentzian and Gaussian component curves after the background subtraction, according to Shirley and Sherwood.

The metal content was measured by inductively coupled plasma (ICP) analysis using an IRIS Advantage spectrometer. The metal dispersions on Pt, Pd and Rh samples were measured by H_2 and CO chemisorptions using a Micromeritics ASAP 2020 instrument [54, 55]. For the H_2 chemisorptions, the samples were first treated in pure H_2 at 623 K (0.067 K s^{-1}) for 1 h and then in a dynamic vacuum at 623 K for 1 h. Hydrogen adsorption isotherms were measured at 313 K and 5.0–50 kPa of H_2 for Pt and Rh. To avoid formation of the b-hydride phase in the Pd samples, the isotherms were measured at 343 K and 0.4–1.5 kPa of H_2.

For CO chemisorption, the catalysts was reduced under pure H_2 atmosphere at 623 K (0.067 K s^{-1}) for 1 h, followed by a dynamic vacuum at the same temperature for 3 h. The catalyst was then brought to 313 K under vacuum. After introducing CO to the sample, adsorption isotherms were measured at 313 K and 5.0–50 kPa. Metal dispersions were calculated using adsorption stoichiometry of $H/Pt_s = 1$, $H/Pd_s = 1$, $H/Rh_s = 1$, $CO/Pt_s = 1$and $CO/Pd_s = 1$.

2.4. Catalytic reactions

The 4-chlorophenol HDC experiments were performed in a 500 mL batch mode three-necked flask under continuous stirring at room temperature and atmospheric pressure. The effect of increasing the H_2 flow rate and stirring speed on the hydrodechlorination performance was investigated, and a hydrogen flow rate of 1 cm^3 s^{-1} and a stirring speed of 600 rpm were set to exclude the limit of H_2 diffusion. In a typical reaction, 0.1~2.0 g of catalyst was transferred into the reactor and treated by a hydrogen flow (1 cm^3 s^{-1}) at 353 K for 1 h to reduce the surface noble metal oxides. Then, the temperature of the reactor was cooled to room temperature (298 K), and deionized water with a trace amount of NaOH (to maintain the pH of the reaction solution at 7) were added under 600 rpm stirring with a 1 cm^3 s^{-1} hydrogen flow. The initial NaOH concentration ([NaOH]) in the reaction mixture was in the range of 0 and 10 mmol L^{-1}, such that the [NaOH]/[4-CP] ratio lies between 0 and 1. After stirring for 10 min, a certain amount of 4-chlorophenol was injected to create a 0.1~10 mmol L^{-1} solution, and the reaction was immediately timed. To evaluate the conversion rate of the reaction, samples were collected with a glass syringe at 2 min intervals and passed through a 0.45 μm membrane filter.

For the 4-CP HDC reaction, a series of blank experiments were conducted in the absence of a catalyst with a preliminary 4-CP concentration (C_0) of 0.5~10 mmol L^{-1} and a hydrogen flow rate of 1 cm^3 s^{-1}. The loss of 4-CP content in the H_2 flow was negligible (<0.1%) in 2 h. The impacts of the hydrogen flow rate, temperature, stirring speed and initial pH on the reaction were also studied, and the reaction conditions were

selected to minimize the transport limitations observed in our previous work [56].

To test the chloride effect, different amounts of NaCl were added to the initial HDC solution to obtain chloride concentrations ranging from 0 to 0.8 mol L^{-1}. To test the sulfide effect, Na_2S was also added to the HDC solution at different ratios of sulfur to surface active Pd, which was similar to the work of Wong et al [30].

The concentration of 4-CP and phenol after the reaction were measured by an HPLC with a diode-array detector using a C_{18} column. Other products (i.e., cyclohexanone) were analyzed by GC (GC-7860) using a 30 m length and 0.25 mm i.d. capillary column (DB-Wax, Agilent) connected to a flame ionization detector.

In many cases, the reactions were tested for repeatability under identical conditions, and the reaction reproducibility was better than ±5%. The carbon balance was calculated by comparing the amount of carbon entering per unit time and the number of products exiting per unit time, and the carbon mass balance was within discrepancy of ±1%. A chlorine (in the form of Cl^- ions in product) mass balance was performed by potentiometric titration with 0.01~0.05 mol L^{-1} $AgNO_3$ solution via a Metrohm Model 905 Autotitrator. The Cl mass balance was complete to better than ±5%.

The turnover rate (TOR) of HDC reaction was reported as the molar conversion rate of 4-CP per surface metal atom. Selectivities were calculated based on the percentage of the converted 4-CP in the product. The residence time (mol surface metal s mol^{-1} reactant) was defined as the reciprocal of the space velocity, which was controlled by varying the reactant molar rates while keeping the respective pressures constant [57].

In this study, the 4-CP-to-catalyst ratio was varied (at the same concentration of 4-CP and hydrogen) to study the effect of conversion on the TOR. The initial TOR was obtained by extrapolation to zero conversion.

3. Results and discussion

3.1. Catalyst properties

Table 1 shows the metal loading and metal dispersion of the SiO_2-supported metals and metal phosphides. With the increase in the metal loading on the SiO_2 supports, the metal dispersion decreases, suggesting the growth of the mean cluster size of the metal and metal phosphide particles. The mean cluster size of the metal and that of the metal phosphide particles were measured via hydrogen and CO chemisorptions, and TEM measurement, respectively. The trends of size variation with metal loading for metal and phosphide particles are similar on all three measurement techniques. In particular, the size of Pd and Pt particles are similar based on chemisorption and TEM results. However, the size of phosphide particle obtained from the TEM images is a slightly larger than the calculated values from chemisorption technique. However, TEM imaging is difficult to distinguish small clusters and the increase of crystal cell parameter caused by the introduction of P into the metal lattice. For instance, the cubic Pd metal crystal can be converted to orthorhombic $Pd_3P_{0.95}$ crystal. In order to obtain a reasonable reaction rate based on the active surface sites of metal, the dispersion from hydrogen chemisorption was adopted and its corresponding mean size of metal and phosphide particles are used to elucidate the structural sensitivity of the HDC reaction.

Fig. 1, S1 and S2 show the XRD patterns of the SiO_2-supported noble metals (Pd, Rh and Pt) and their corresponding phosphides ($Pd_3P_{0.95}$, Rh_2P and PtP_2). The XRD pattern (Fig. 1a) of the Pd/SiO_2 sample has three reflection peaks at 2θ=40.4°, 46.8° and 68.4°, which correspond to the Pd (111), (200) and (200) lattice planes, respectively; these results indicate the formation of metallic palladium compounds (JCPDS No. 1-1201). The XRD pattern (Fig. 1a) of the palladium phosphide with 10 wt. % Pd loading only contains peaks that are characteristic of $Pd_3P_{0.95}$ compounds (JCPDS No. 1-089-3046), whereas the sample with a lower Pd loading (5 wt. %) contains broad peaks at approximately 2θ=35°~45° because of the small size and homogeneous distribution of the $Pd_3P_{0.95}$ particles, which was confirmed by the TEM and hydrogen chemisorptions results (see discussion below). Fig. S1 shows the formation of metallic rhodium (JCPDS No. 1-1214), Rh_2P compounds (JCPDS No. 2-1299), metallic platinum (JCPDS No. 1-1194) and PtP_2 compounds (JCPDS No. 1-071-2233) on the SiO_2-supported rhodium, rhodium phosphide, platinum and platinum phosphide samples, respectively. These data indicate that the crystalline noble metals (Pd, Rh and Pt) and their corresponding phosphides ($Pd_3P_{0.95}$, Rh_2P and PtP_2) were successfully synthesized by the temperature-programmed reduction with hydrogen without the introduction of other phosphating agents (e.g., PH_3).

The morphology and size of palladium phosphide particles with different Pd loadings (1, 5 and 10 wt. %) on SiO_2 were inspected by TEM, as shown in Fig. 2 and S2. The palladium phosphides have spherical particles and the particle size increased

as the metal loading increased from 1 to 10 wt. %. Notably, the phosphide particles on the supported palladium phosphide sample with 1 wt. % Pd loading (Fig. S2) were difficult to distinguish because of the small particle size and high dispersion of the particles (0.96 Pd dispersion according to the hydrogen chemisorption characterization, Table 1 entry 8). Approximately 5 nm palladium phosphide particles were observed on the sample with 5 wt. % Pd loading, which is consistent with the hydrogen chemisorption results (5.3 nm mean cluster size calculated based on the 0.21 palladium dispersion, Table 1 entry 11). However, a broad size distribution (5~20 nm) of palladium phosphide particles was found for the sample with a 10 wt.% metal loading, which suggested a low metal dispersion (0.08, Table 1 entry 13). These data agreed with the increase in the intensity of the diffraction peaks corresponding to the $Pd_3P_{0.95}$ compounds in the XRD patterns of the supported palladium phosphide samples as the Pd loading increased from 5 to 10 wt. % (Fig. 1).

To further investigate the surface structural and electronic properties of the SiO_2-supported Pd and $Pd_3P_{0.95}$ samples, XPS measurements were conducted, and the results are illustrated in Fig. 3 and 4 and Table 2 and 3. Table 2 and 3 include the XPS data of the Pd binding energies and surface atomic ratios for the catalysts before and after hydrodechlorination. Fresh Pd/SiO_2 (Fig. 3) displays peaks at 341.0 eV that correspond to Pd^0 $3d_{3/2}$ and bands at 335.7 eV that correspond to Pd^0 $3d_{5/2}$. In comparison to the Pd/SiO_2 peaks, both the peaks in $Pd_3P_{0.95}/SiO_2$ slightly increase to 341.2 and 335.9 eV. This may be attributed to the transfer of electrons from the Pd species to P species, which has been reported for amorphous metal-phosphor nanoparticles [58]. It should

be noted that the small binding energy shift (less than 0.2 eV) could be attributed to analytical error. In order to show the interaction between Pd and P species, the FT-IR spectra of CO adsorption was obtained (Fig. S3). Two absorption bands at 1964 cm^{-1} (CO mainly on the Pd bridging sites) and 2089 cm^{-1} (CO occupying the Pd atop sites) are given by the Pd/SiO_2. On the other hand, the bands associated with the CO adsorption on the Pd atop sites in $Pd_3P_{0.95}/SiO_2$ were shifted from 2089 cm^{-1} and 1964 cm^{-1} to 2072 $cm^{-1}$and 1952 cm^{-1}, respectively, indicating an obvious influence from the ligand through changing the chemical environment around the Pd atoms.

After the introduction of P into Pd metal, the binding energy of the P species in $Pd_3P_{0.95}/SiO_2$ is 133.1 eV, which corresponds to the energy of PO_4^{3-} groups. Moreover, a high atomic ratio of P to Pd at approximately 12 was determined from the surface composition (Table 3). This suggests that the surface of $Pd_3P_{0.95}/SiO_2$ is rich in phosphates which agreed with the report that the surface of the phosphides synthesized via the temperature-programmed reduction method with excess phosphate (i.e., $NH_4H_2PO_4$) is always covered by phosphate [59].

After the HDC reaction, the binding energies of the Pd species in Pd/SiO_2 (Fig. 3) slightly increase from 340.9 and 335.6 eV to 341.4 and 336.2 eV, respectively. Fig. 4 and Table 2 and 3 show the formation of surface Cl^- species on the Pd/SiO_2. These results indicate the interaction of Cl and Pd metal via the transfer of electrons from Pd to Cl species. Unlike Pd/SiO_2, $Pd_3P_{0.95}/SiO_2$ possesses slight growth (~0.1 eV) in the binding energies of the Pd species. However, the binding energy of P species (Fig. 4

and Table 2) changes from 133.1 eV (for P^{5+} species) to 131.1 eV (for P^0 species), and the surface concentration decreases (7.01×10^{-2} to 0.21×10^{-2} atomic ratio of P/O, Table 3). The sharp decrease in the surface concentration of P species should be due to the dissolution of surface phosphate in water, and the surface atomic ratio of Pd/P becomes 3.2, which is similar to the bulk composition of $Pd_3P_{0.95}$. Interestingly, few Cl species were observed on $Pd_3P_{0.95}/SiO_2$ after HDC reaction. Accordingly, the introduction of P to the Pd lattice to form $Pd_3P_{0.95}$ inhibits the sorption of Cl^- ions. In addition, the phosphide catalyst could be the stable catalyst in the HDC reaction even the presence of poison species (i.e., S^{2-} for metal catalysts). For the Pd/SiO_2 samples treated in Na_2S solution, a new binding energy at 337.1 eV is observed (attributed to Pd^{2+} in the palladium sulfide compounds) (Fig. 3), suggesting the surface reaction of S^{2-} and the metallic Pd sites. The XPS spectra of S species (Fig. 4 and Table 3) confirm the surface is rich in S^{6+} (corresponding to the peaks at 168.1 eV) species, which form via the oxidation of S^{2-} to $S_2O_3^{2-}$ species during the drying process of the treated samples in air prior to XPS characterization. In contrast, the $Pd_3P_{0.95}/SiO_2$ sample still shows a shift in the binding energy (~0.2 eV) compared to the fresh catalyst. An obvious change in the shift of the binding energy (from 133.1 to 133.8 eV) for the P species is observed and may be due to the formation of surface phosphorus-sulfur compounds. Strangely, the sulfur compound is difficult to detect. These data show that $Pd_3P_{0.95}/SiO_2$ possesses good resistance to Cl^- and S^{2-} ions in aqueous solutions and is a potential stable catalyst for the aqueous HDC reaction.

3.2 HDC activity of the noble metal and phosphide catalysts

The pseudo-first-order kinetics is selected for the aqueous-phase HDC of 4-CP over the noble metal catalysts [5-25]:

$$\frac{dc}{dt} = -k_{obs}C \qquad (1)$$

where C is the 4-CP concentration (mol L^{-1}) in the solution phase and k_{obs} (min^{-1}) is the observed pseudo-first-order reaction rate constant. The rate constants were obtained from a linear regression of the natural log of the solution phase concentration versus time [5, 56]. Fig. S3 and S4 and Table S2 show that the palladium and rhodium phosphide catalysts also follow pseudo-first-order kinetics.

Fig. 5 shows the product distribution of the 4-CP HDC reaction for different reaction conversions. Only phenol and cyclohexanone organic compounds were detected in our experiments, which suggested cyclohexanone was not hydrogenated to cyclohexanol over the Pd-based catalysts [6]. The selectivity of phenol decreases with the conversion while the selectivity of cyclohexanone increases. Interestingly, a higher selectivity of cyclohexanone was observed on palladium than the palladium phosphide catalyst, which indicated the better hydrogenation capability of the aromatic rings via the metallic surface rather than the phosphide surface. However, the selectivity of phenol is still much higher than that of cyclohexanone. This represents a difficulty in the hydrogenation of aromatic rings.

The initial turnover rate was estimated based on the common rate analysis technique using the extrapolation of the conversion to zero residence time (the reciprocal of the space velocity) [57]. Given the turnover rate or the conversion is a

function of residence time, the hypothetical rate at zero conversion can be taken as the initial turnover rate. For the liquid HDC reaction, we used different ratios of 4-CP to catalyst (at the same concentration of 4-CP and hydrogen) to study the effect on the turnover rate. This is equivalent to the effect of space velocity on conversion in gas-phase heterogeneous catalytic reactions. We used the plot of turnover rate as a function of conversion to approximate the initial turnover rate of HDC via extrapolation to zero conversion. The initial turnover rates (TOR) obtained in Fig. 5b and Table 1 were used to discuss the activity and reaction pathways of the 4-CP HDC reactions.

Among the Pd, Rh and Pt nanoparticles, which have similar particle size of 5~8 nm, on SiO_2 (Fig. 6 and Table 1), the Pd/SiO_2 and Rh/SiO_2 samples gave the highest and lowest initial TOR values of 1.25 $\times 10^{-4}$ mol $mol_{surf\text{-}Pd}^{-1}$ s^{-1} and 0.57 $\times 10^{-4}$ mol $mol_{surf\text{-}Pd}^{-1}$ s^{-1}, respectively. This result shows that Pd metal is a more suitable choice among other noble metal catalysts, which is in agreement with the work reported by Diaz et al [60]. Unlike a higher activity given by Rh/Al_2O_3 over Pt/Al_2O_3 [60], it should be noted that the TOR value of our synthesized Rh/SiO_2 catalysts (0.46~0.57 $\times 10^{-4}$ mol $mol_{surf\text{-}Pd}^{-1}$ s^{-1}) is slightly lower than that of our synthesized Pt/SiO_2 catalysts (0.55~0.78 $\times 10^{-4}$ mol $mol_{surf\text{-}Pd}^{-1}$ s^{-1}). Molina et al reported an activity order for pillared clays-supported Pt, Pd and Rh catalysts: Rh>Pd>Pt [21]. It is possible that the HDC activity on Rh and Pd catalysts were improved by the metal-support interactions in pillared clay and Al_2O_3 [21, 60], which is different from our system using SiO_2 as a support. For the phosphide nanoparticles with a size of 5~8 nm, $Pd_3P_{0.95}/SiO_2$ gave a TOR value of 1.36 $\times 10^{-4}$ mol $mol_{surf\text{-}Pd}^{-1}$ s^{-1}, which is higher than that of Rh_2P/SiO_2 (0.97 $\times 10^{-4}$ mol $mol_{surf\text{-}}$

$_{Pd}^{-1}$ s^{-1}) and PtP_2/SiO_2 (0.72×10^{-4} mol $mol_{surf\text{-}Pd}^{-1}$ s^{-1}). Interestingly, Bussell et al. reported a higher hydrodesulfurization turnover frequency on Rh_2P/SiO_2 over Pd_5P_2/SiO_2 [46, 48]. In this work, palladium phosphide ($Pd_3P_{0.95}/SiO_2$) is found to be more reactive than the other metal phosphide catalysts in the aqueous HDC reaction of 4-CP.

Fig. 6 shows the effect of the particle size of the metal and phosphide nanoparticles on the initial TOR value. Both Pd/SiO_2 and $Pd_3P_{0.95}/SiO_2$ show similar trends. The initial TORincreases with the particle size for particles smaller than ~8 nm and decreases slightly with enlarging particles. These data show that the structural sensitivity could be a determining factor to the HDC reactivity, which is consistent with the results reported by Diaz et al. [10, 20, 27, 38]. It is proposed that the rate-limiting step of the HDC reaction is the C–Cl hydrogenolysis of the adsorbed molecule [61, 62], which is catalyzed by the surface palladium atoms. In HDC of chlorophenol, the hydroxyl group of chlorophenol increases the electron density within the ring via an inductive effect and, hence, activates the aromatic ring for electrophilic attack. 4-chlorophenol possesses multiple bonds that can be chemisorbed on the metal surface through π-bonding, involving donation of π-electron density from the adsorbate towards the metal surface which requires large ensemble. The probability of forming such an ensemble increases with increasing nanoparticle size, which leads to an increase in the initial TOR. The number of atoms surrounding each surface metal atom decreases with decreasing particle size; affecting the nature and strength of the interactions between the surface of metal particles and 4-CP molecules [10, 20]. Therefore, the

change in the coordination associated with the nanoparticle size has a strong effect on the adsorption energy. In general, smaller particles contain more surface atoms on the edges of the crystallographic planes or on the edge junctions. They tend to increase the number of active sites that are accessible to the 4-CP molecules [63]. These factors indicate that an optimum particle size is expected for the HDC reaction and that the particles must possess a sufficient ensemble to adsorb and activate 4-CP. Metal particles with a large particle size and a high coordination number attends to give low reactivity. For particles larger than 10 nm, however, $Pd_3P_{0.95}/SiO_2$ exhibits a slightly lower activity than the Pd/SiO_2 catalyst. Here, geometric or ensemble effects emerge because of the dilution of the surface active metal (Pd) by an inactive one (P). However, the presence of P changes the valence of the surface Pd species and inhibits the interaction between Pd and Cl^- ions, as shown in the XPS results. As a result, both electronic and geometric effects should be considered when screening the particle size of $Pd_3P_{0.95}/SiO_2$. Based on the results, it is concluded that a size of ~5 nm and ~8 nm is suitable for $Pd_3P_{0.95}/SiO_2$ and Pd/SiO_2, respectively.

3.3 Kinetic modeling and the effect of chloride on the HDC reaction rate

In the XPS results, different contents of Cl^- species are observed on $Pd_3P_{0.95}/SiO_2$ and Pd/SiO_2 after the HDC reaction (Fig. 4 and Table 3), and thus, the effect of the sorption of Cl^- species on Pd/SiO_2 should be more important than that on $Pd_3P_{0.95}/SiO_2$ for the HDC reaction. Here, we attempted to explore the kinetic model of the HDC of 4-CP based on the Langmuir-Hinshelwood (L-H) mechanism to clarify the difference.

For the L-H mechanism, the rate-determining step of the HDC reaction is regarded to be the C–Cl hydrogenolysis of the 4-CP reaction with H atoms on metal surface [6, 43, and 44]. Here, Fig. 7 presents the elementary steps of the 4-CP HDC reaction over the palladium and palladium phosphide catalysts.

As shown in Fig. 7, 4-CP and hydrogen adsorb onto the catalyst surface to form M-CP and M-H, which are the most abundant reactive intermediates, via quasi-equilibrium reactions. The quasi-equilibrium assumption requires fast 4-CP and H adsorption-desorption processes on the time scale of the kinetically relevant molecular or ion-adsorption events. However, the hydrogen chemisorbed by the Pd metal is in the lattice of the surface metal crystal. Here, all the palladium-based catalysts were reduced by hydrogen prior to the HDC reaction, which suggested a hydrogen-rich surface and the formation of surface PdH_x compounds [6-25]. Thus, the equilibrium adsorption of 4-CP and hydrogen should not be competitive.

The surface coverages (θ_i, i= 4-CP, phenol, cyclohexanone, HCl, and Cl^-) of the adsorbed species for the steps (1.1~1.9) are given by the Langmuir adsorption isotherms. Because NaOH was present in the initial solution to maintain a pH value higher than 7, HCl compounds should be consumed as soon as they are formed. Moreover, a much lower selectivity for cyclohexanone than phenol, as shown in Fig. 5, suggests the low hydrogenation activity of the aromatic ring on the Pd catalysts. Thus, we assumed the sorption of HCl and cyclohexanone could be ignored compared to the sorption of other species.

$$\theta_{MCP} = \frac{K_{CP}[4-CP]}{1+K_{CP}[4-CP]+K_{Cl}[Cl^-]+K_{Ph}[Ph]} \quad (2)$$

The HDC turnover rate can be written as:

$$r = k_1[MCP][MH] = \frac{k_1 K_{CP}[4-CP]}{1+K_{CP}[4-CP]+K_{Cl}[Cl^-]+K_{Ph}[Ph]} \times [MH] = \frac{kK_{CP}[4-CP]}{1+K_{CP}[4-CP]+K_{Cl}[Cl^-]+K_{Ph}[Ph]} \quad (3)$$

where $k=k_1 \times [MH]$.

At the beginning of the reaction, the kinetic model can be expressed as:

$$r_0 = \frac{kK_{CP}[4-CP]_0}{1+K_{CP}[4-CP]_0} \quad (4)$$

where r_0 (mol $mol_{surf\text{-}Pd}^{-1}$ s^{-1}) is the initial TOR value, $[4\text{-CP}]_0$ is the initial $[4\text{-CP}]_0$ concentration (mol L^{-1}), and k (mol $mol_{surf\text{-}Pd}^{-1}$ s^{-1}) is the intrinsic rate constant.

To test the kinetic model and investigate the relative contribution of the 4-CP adsorption and surface reaction to the HDC reaction, the influence of the 4-CP initial concentration was evaluated (Fig. 8a). The initial reaction rate was measured for various initial 4-CP concentrations from 0.05 to 10 mmol L^{-1}. r_0 increases with the increase in the initial 4-CP concentration for the palladium and palladium phosphide catalysts in the order of $Pd_3P_{0.95}/SiO_2$ > Pd/SiO_2 over the entire range of the tested concentrations (Fig. 8a). The L-H model (Equation (4)) well fits the initial TOR value versus the initial concentration (R^2>0.99, Table 4). A higher intrinsic rate constant k and equilibrium adsorption constant, K_{CP}, were obtained for $Pd_3P_{0.95}/SiO_2$ than the Pd/SiO_2 catalysts. This agrees with the electronic properties of the $Pd_3P_{0.95}$ particles determined by the XPS characterization; i.e., Pd electron transfer to P and 4-CP is preferable to Pd site adsorption.

The reactivity of the $Pd_3P_{0.95}/SiO_2$ and Pd/SiO_2 catalysts were further tested in

aqueous solutions with varying concentrations of NaCl from 0 to 0.8 mol L^{-1} at pH 7. The kinetic model can be expressed as:

$$r_0 = \frac{kK_{CP}[4-CP]_0}{1+K_{CP}[4-CP]_0+K_{Cl}[Cl^-]_0} \quad (5)$$

The results show a decrease in the rate constant of Pd/SiO_2 compared with that of $Pd_3P_{0.95}/SiO_2$ (21% decrease vs. 10% decrease in the initial TOR value, Fig. 8b) when the NaCl concentration increases from 0 to 0.8 mol L^{-1}. Both $Pd_3P_{0.95}/SiO_2$ and Pd/SiO_2 show a similar trend for the change in the initial TOR value; i.e., a faster decrease in the rate is observed from 0 to 0.1 mol L^{-1} followed by a marginal change upon further increases in the NaCl concentration. The L-H model (Equation (5)) well fits the initial TOR value versus the initial concentration of Cl ions (R^2>0.99, Table 4). A much lower equilibrium adsorption constant, K_{Cl}, was obtained for $Pd_3P_{0.95}/SiO_2$ than Pd/SiO_2 catalysts, which confirms the result that few Cl elements could be detected on the surface of $Pd_3P_{0.95}/SiO_2$ after the HDC reaction. The parity plots in Fig. S7 compares the calculated and the measured initial turnover rates for the HDC at 303 K over Pd/SiO_2 and $Pd_3P_{0.95}/SiO_2$. The plots show good correlation, indicating that Equation (5) describes the measured initial turnover rates accurately for the Pd/SiO_2 and $Pd_3P_{0.95}/SiO_2$. These data show that the 4-CP HDC mechanism followed the typical Langmuir-Hinshelwood mechanism as reported by previous works [5, 64, 65]. That is, both 4-CP and hydrogen are first adsorbed on the metal surface, followed by their activation and reaction that produces phenol and Cl adsorbed on the metal surface.

3.4 The effect of sulfide on the HDC reaction rate

Fig. 8c shows the results for the sulfide poisoning experiments on the SiO_2-supported Pd and $Pd_3P_{0.95}$, and the sulfide-to-surface Pd atom ratios were considered. In the absence of sulfide, the $Pd_3P_{0.95}/SiO_2$ and Pd/SiO_2 catalysts had initial TOR values of 1.36 and 1.25 mol $mol_{surf\text{-}Pd}^{-1}$ s^{-1}, respectively. The 4-CP HDC activities of the $Pd_3P_{0.95}/SiO_2$ and Pd/SiO_2 catalysts monotonically decreased with the addition of sulfide, but the addition of sulfide had little effect on the $Pd_3P_{0.95}/SiO_2$ and Pd/SiO_2 catalysts until $S:Pd_{surf}$ ratios of 0.8 and 1.0, respectively. As a result, the addition of sulfide at a $S:Pd_{surf}$ ratio >1.0 decreased the initial HDC TOR value to ~0.7 of its value prior to the sulfide addition on $Pd_3P_{0.95}/SiO_2$ and fully suppressed the rate on Pd/SiO_2 (~0.1 of its original value). This small decrease in the HDC ratio on the phosphide catalysts reflects either the competitive sorption between 4-CP and sulfide on the phosphide surface or irreversible sulfide poisoning of the metal sites with low coordination numbers [30]. The introduction of P apparently enhances the sulfide poisoning resistance of Pd for the 4-CP HDC reaction. This beneficial presence of phosphide was observed in gas-phase HDS reactions using phosphides [44, 59]. The phosphides formed shows a good sulfur or sulfide resistance which prevents bulk formation of catalytically inactive Pd_4S crystallites, as shown in Fig. S6. Hayes et al. proposed that bonding in noble metal phosphide (i.e., Rh_2P) is dominated by metal-P (i.e., Rh-P) interactions, as indicated by the metal-P distance (i.e., Rh-P, 0.2381 nm) that is shorter than the metal-metal distance (Rh-Rh, 0.2749 nm) [46]. Thus, the sulfur/sulfide resistance in the noble metal phosphide catalyst is likely attributed to the

P in the phosphide particles. They inhibit the irreversible adsorption of S at the particle surface and avoid possible incorporation of S into the bulk phase (i.e. prevent formation of noble metal sulfide) [46-48].

3.5 Catalyst stability

To determine the stability of the Pd-based catalysts, the $Pd_3P_{0.95}/SiO_2$ and Pd/SiO_2 catalysts were recycled for the 4-CP HDC reaction. For each recycling experiment, the catalysts were collected and sequentially washed with water and ethanol and dried in vacuum prior to use. The $Pd_3P_{0.95}/SiO_2$ catalysts exhibited stability over the first six recycles based on the initial TOR value data (3% decrease), whereas an obvious decrease (11%) in the TOR values of the Pd/SiO_2 catalysts was observed. According to previous studies [30, 42, 43], catalyst deactivation mainly occurs due to the chemisorption of chloride onto active sites and leaching and sintering of active sites. In our study, the ICP and chemisorption results exclude the leaching and sintering problems of the Pd/SiO_2 and $Pd_3P_{0.95}/SiO_2$ catalysts. Moreover, the $Pd_3P_{0.95}/SiO_2$ catalysts exhibited a better capacity to resist poisoning than the Pd catalysts, which can be attributed to the presence of P species.

4. Conclusion.

$Pd_3P_{0.95}/SiO_2$, Rh_2P/SiO_2 and PtP_2/SiO_2 catalysts were prepared via a temperature-programmed reduction and were utilized for aqueous-phase HDC of 4-CP under mild

reaction conditions (298 K). $Pd_3P_{0.95}/SiO_2$ was shown to be the most active phosphide catalyst. The Pd/SiO_2 catalysts show an obvious decrease in the HDC rate in the presence of chloride because of Cl chemisorption onto Pd metal sites. The introduction of P into the metallic lattice of the Pd/SiO_2 catalysts changes the valence of the Pd atoms. The surface interactions between Pd and P species promote the adsorption of 4-CP but inhibit the sorption of Cl ions after the HDC reaction, which was shown in the XPS characterization and kinetic study results. The Pd/SiO_2 catalysts were almost inactive (90% decrease in the TOR value) at a $S:Pd_{surf}$ ratio of 1, while the $Pd_3P_{0.95}/SiO_2$ catalyst possesses a better sulfide poisoning resistance (30% decrease in the TOR value). This improved sulfide resistance was related to the protection of the Pd active site from the formation of the Pd_4S compounds via the formation of a phosphide structure. The HDC of 4-CP over $Pd_3P_{0.95}/SiO_2$ catalysts is a structure-sensitive reaction, and the electronic and ensemble effects of the palladium phosphide particles determine the initial TOR. $Pd_3P_{0.95}/SiO_2$ catalysts can be the basis for highly active and highly stable catalysts for groundwater treatment applications.

Acknowledgements

The present work was supported by the Natural Science of Foundation China (U1662131, 21206192 and 21576140), 111 project B12015, and the Science Foundation of China University of Petroleum-Beijing (C201603).

Supplementary material

Experimental details on the XRD and TEM characterizations of the catalysts and the kinetic study of the catalysts.

References

[1] M. A. Keane, , ChemCatChem 3 (2011) 800-821.

[2] F. Alonso, I. P. Beletskaya, M. Yus, Chem. Rev. 102 (2002) 4009-4091.

[3] I. Ali, V.K. Saini, Environ. Sci. Technol. 38 (2004) 4012–4018.

[4] M. A. Keane, J. Chem. Technol. Biotechnol. 80 (2005) 1211-1222.

[5] N. Jadbabaei, T. Ye, D. Shuai, H. Zhang, Appl. Catal. B 205 (2017) 576-586.

[6] C. B. Molina, A. H. Pizarro, J. A. Casas, J. J. Rodriguez, Appl. Catal. B 148-149 (2014) 330-338.

[7] M. Munoz, Malte Kaspereit, B. J. M. Etzold, Chem. Eng. J. 285 (2016) 228-235.

[8] V. Felis, C. D. Bellefon, P. Fouiloux, D. Schweich, Appl. Catal. B., 20 (1999) 91-100

[9] Y. Shindler, Y. Matatov-Meytal, M. Sheintuch, Ind. Eng. Chem. Res., 40 (2001) 3301-3308

[10] J. A. Baeza, L. Calvo, D. Y. Murzin, J. J. Rodriguez, M. A. Gilarranz, Catal. Lett. 144 (2014) 2080-2085

[11] X. Ma, Y. Liu, X. Li, J. Xu, G. Gu, C. Xia, Appl. Catal. B 165 (2015) 351-359.

[12] G. Yuan, M. A. Keane, Catal. Commun. 4 (2003) 195-201.

[13] G. Yuan, M. A. Keane, Catal. Today 88 (2003) 27-36.

[14] G. Yuan, M. A. Keane, Appl. Catal. B 52 (2004) 301-314.

[15] G. Yuan, M. A. Keane, J. Catal. 225 (2004) 510-522.

[16] H. M. Roy, C. M. Wai, T. Yuan, J. K. Kim, W. D. Marshall, Appl. Catal. A 271 (2004) 137-143.

[17] L. Calvo, A. F. Mohedano, J. A. Casas, M. A. Gilarranz, J. J. Rodriguez, Carbon 42 (2004) 1377-1381.

[18] L. Calvo, M. A. Gilarranz, J. A. Casas, A. F. Mohedano, J. J. Rodríguez, Appl. Catal. B 67 (2006) 68-76.

[19] C. Xia, Y. Liu, S. Zhou, C. Yang, S. Liu, S. Guo, Q. Liu, J. Yu, J. Chen, Catal. Commun. 10 (2009) 1443-1445.

[20] J. A. Baeza, L. Calvo, M. A. Gilarranz, A. F. Mohedano, J. A. Casas, J. J. Rodriguez, J. Catal. 293 (2012) 85-93.

[21] Z. M.de Pedro, E. Diaz, A. F. Mohedano, J. A. Casas, J. J. Rodriguez, Appl. Catal. B 103 (2011) 128-135.

[22] L. Cheng, Z. Jin, X. Wang, Catal. Commun. 41 (2013) 60-64.

[23] J. Zhou, K. Wu, W. Wang, Z. Xu, H. Wan, S. Zheng, Appl. Catal. A 470 (2014) 336-343.

[24] H. Deng, G. Fan, C. Wang, L. Zhang, Catal. Commun. 46 (2014) 219-223.

[25] Z. Dong, C. Dong, Y. Liu, X. Le, Z. Jin, J. Ma, Chem. Eng. J. 270 (2015) 215-222.

[26] A. H. Pizarro, C. B. Molina, J. L. G. Fierro, J. J. Rodriguez, Appl. Catal. B 197 (2016) 236-243.

[27] E. Diza, A. F. Mohedano, J. A. Casas, L. Calvo, M. A. Gilarranz, J. J. Rodriguez, Appl. Catal. B 106 (2011) 469-475.

[28] M. Munoz, Z. M. De Pedro, J. A. Casas, J. J. Rodriguez, Appl. Catal. A 488 (2014) 78-85.

[29] J. A. Baeza, L. Calvo, M. A. Gilarranz, J. J. Rodriguez, Chem. Eng. J. 240 (2014) 271-280.

[30] K. N. Heck, M. O. Nutt, P. Alvarez, M. S. Wong, J. Catal. 267 (2009) 97-104.

[31] P. D. Vaidya, V. V. Mahajani, Appl. Catal. B 51 (2004) 21-31.

[32] J. J. Wei, X. H. Xu, Y. Liu, D. H. Wang, Water Res. 40 (2006) 348-354.

[33] J. A. Baeza, L. Calvo, J. J. Rodriguez, E. Carbo-Argibay, J. Rivas, M. A. Appl. Catal. B 168-169 (2015) 283-292.

[34] C. Xia, Y. Liu, J. Xu, J. Yu, W. Qin, X. Liang, Catal. Commun., 10 (2009) 456-458

[35] C. Xia, Y. Liu, J. Xu, J. Yu, W. Qin, X. Liang, Catal. Commun., 10 (2009) 456-458.

[36] C. Ruiz-Garcia, F. Heras, N. Alonso-Morales, L. Calvo, J. J. Rodriguez, M. A. Gilarranz, Catal. Sci. Technol., 8 (2018) 2598-2605.

[37] Y. Lan, L. Yang, M. Zhang, W. Zhang, S. Wang, ACS Appl. Mater. Interface, 2 (2010) 127-133.

[38] M. Munoz, S. Ponce, G. R. Zhang, B. J. M. Etzold, Appl. Catal. B, 192 (2016) 1-7

[39] E. J. Shin, M. A. Keane, React. Kinet. Catal. Lett. 69 (2000) 3-8.

[40] J. W. da-Silva, R. E. Bruns, A. J. G. Cobo, Chem. Eng. J. 131 (2007) 59-64.

[41] M. Munoz, G. R. Zhang, B. J. M. Etzold, Appl. Catal. B, 203 (2017) 591-598.

[42] D. Angeles-Wedler, K. Mackenzie, F. –D. Kopinke, Environ. Sci. Technol. 42 (2008) 5734-5739.

[43] E. Lopez, S. Ordonez, F. V. Diez, Appl. Catal. B 62 (2005) 57-65.

[44] Y. K. Lee, S. T. Oyama, Appl. Catal. A 548 (2017) 103-113.

[45] R. H. Bowker, M. C. Smith, B. A. Carrillo, M. E. Bussell, Top. Catal. 55 (2012) 999-1009.

[46] J. R. Hayes, R. H. Bowker, A. F. Gaudette, M. C. Smith, C. E. Moak, C. Y. Nam, T. K. Pratum, M. E. Bussell, J. Catal., 276 (2010) 249-258.

[47] Y. Kanda, Y. Matsukura, A. Sawada, M. Sugioka, Y. Uemichi, Appl. Catal. A, 515 (2016) 25-31.

[48] G. H. L. Savithra, R. H. Bowker, B. A. Carrillo, M. E. Bussell, S. L. Brock, ACS Appl. Mater. Interfaces, 5 (2013) 5403-5407.

[49] Y. Kanda, K. Kawanishi, T. Tsujino, A. M. Al-otaibi, Y. Uemichi, Catalysts, 8 (2018) 160.

[50] Y. Shi, B. Zhang, Chem. Soc. Rev. 45 (2016) 1529-1541.

[51] X. Liu, J. Chen, J. Zhang, Ind. Eng. Chem. Res. 47 (2008) 5362-5368

[52] J. Chen, S. Zhou, D. Ci, J. Zhang, R. Wang, J. Zhang, Ind. Eng. Chem. Res., 48 (2009) 3812-3819.

[53] J. A. Cecilia, A. Infantes-Molina, E. Rodríguez-Castellón, A. Jiménez-López, J. Hazard. Mater. 260 (2013) 167-175.

[54] Z. J. Wu, G. Sarika, M. Choi, E. Iglesia, J. Catal. 311 (2014) 458-468.

[55] N. Mahata, V. Vishwanathan, J. Catal., 196 (2000) 262-170.

[56] C. X. Sun, Z. J. Wu, Y. Z. Mao, X. Q. Yin, L. Y. Ma, D. H. Wang, M. H. Zhang, Catal. Lett. 141 (2011) 792-798.

[57] H. Wang, E. Iglesia, J. Catal. 273 (2010) 245-256.

[58] H. Li, H. X. Li, W. L. Dai, W. J. Wang, Z. G. Fang, J. F. Deng, Appl. Surf. Sci. 152 (1999) 25-34.

[59] R. Prins, M. E. Bussell, Catal. Lett. 142 (2012) 1413-1436.

[60] E. Diaz, J. A. Casas, A. F. Mohedano, L. Calvo, M. A. Gilarranz, J. J. Rodriguez, Ind. Eng. Chem. Res. 47 (2008) 3840-3846.

[61] K. Early, V. I. Kovalchuk, F. Lonyi, S. Deshmukh, J. L. d'Itri, J. Catal. 182 (1999) 219-227.

[62] A. L. D. Ramos, M. Schmal, D. A. G. Aranda, G. A. Somorjai, J. Catal. 192 (1999) 423-431.

[63] A. Yu. Stakheev, I. S. Mashkovskii, G. N. Baeva, N. S. Telegina, Russ. J. Gen. Chem., 80 (2010) 618-629.

[64] B. Coq, G. Ferrat, F. Figueras, J. Catal. 101 (1986) 434–445.

[65] I.F. Cheng, Q. Fernando, N. Korte, Environ. Sci. Technol. 31 (1997) 1074–1078.

Figure Captions

Fig. 1 XRD patterns of the SiO_2-supported palladium and palladium phosphide samples..

Fig. 2 The TEM images of the SiO_2-supported palladium phosphides with 5 and 10 wt. % Pd loading.

Fig. 3 XPS spectra of the Pd species on SiO_2-supported Pd and $Pd_3P_{0.95}$ samples with 5 wt. % Pd loading.

Fig. 4 XPS spectra of P, Cl and S species on SiO_2-supported Pd and $Pd_3P_{0.95}$ samples with 5 wt. % Pd loading.

Fig. 5 (a) Product distribution of the 4-CP HDC reaction over the palladium and palladium phosphide catalysts and (b) the effect of the reaction conversion rate on the turnover rate (TOR) of the HDC reaction over the palladium and palladium phosphide catalysts (Initial TOR value, extrapolated to zero conversion (298 K, 3.1 mmol L^{-1} 4-CP)).

Fig. 6 Effect of the metal and phosphide catalyst cluster size on the initial TOR value for the 4-CP HDC reaction (298 K, 3.1 mmol L^{-1} 4-CP)).

Fig. 7 Proposed reaction pathways for the 4-CP HDC Pd-based catalysts (M is a metal surface site, $\rightleftharpoons$ denotes a quasi-equilibrated step, and k_x and K_x are the kinetic and equilibrium constants, respectively, for the individual elementary steps; 4-CP is 4-chlorophenol, Ph is phenol, and one is cyclohexanone.)

Fig. 8 Influence of (a) the initial 4-CP concentration, (b) the initial Cl^- ion concentration and (c) the initial S^{2-} ion concentration on the initial TOR of the HDC reaction (298 K,

3.1 mmol L^{-1} 4-CP, Pd-based catalysts with 5 wt.% metal loading as shown in entries 4 and 11 in Table 1).

Fig. 9 The initial TOR value of the HDC reaction of 4-CP over Pd-based catalysts with 5 wt.% metal loading (entry 4 an 11 shown in Table 1) during the recycle runs.

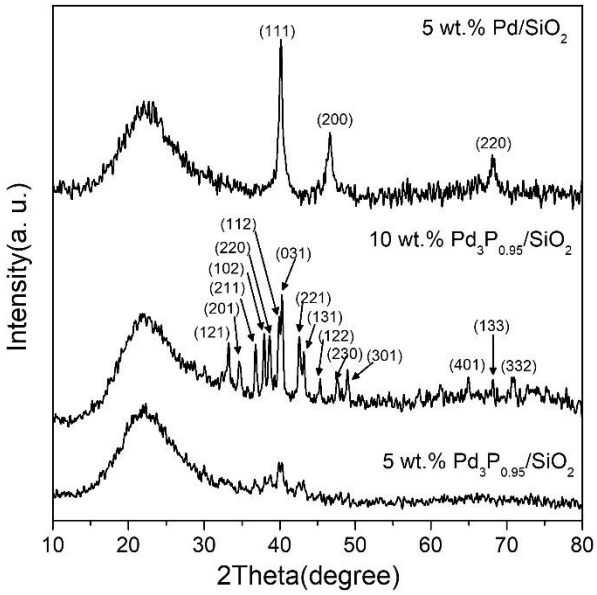

Fig. 1 XRD patterns of the SiO_2-supported palladium and palladium phosphide samples.

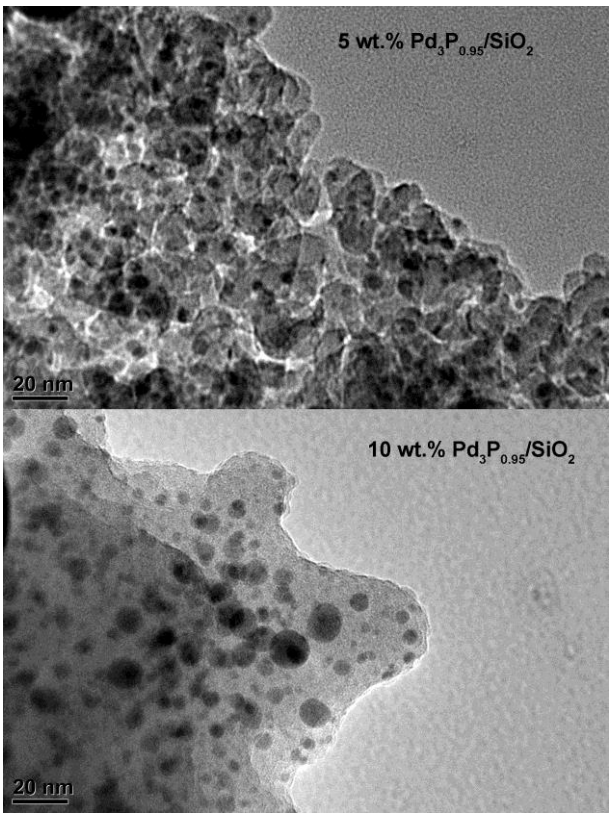

Fig. 2 The TEM images of the SiO_2-supported palladium phosphides with 5 and 10 wt. % Pd loading.

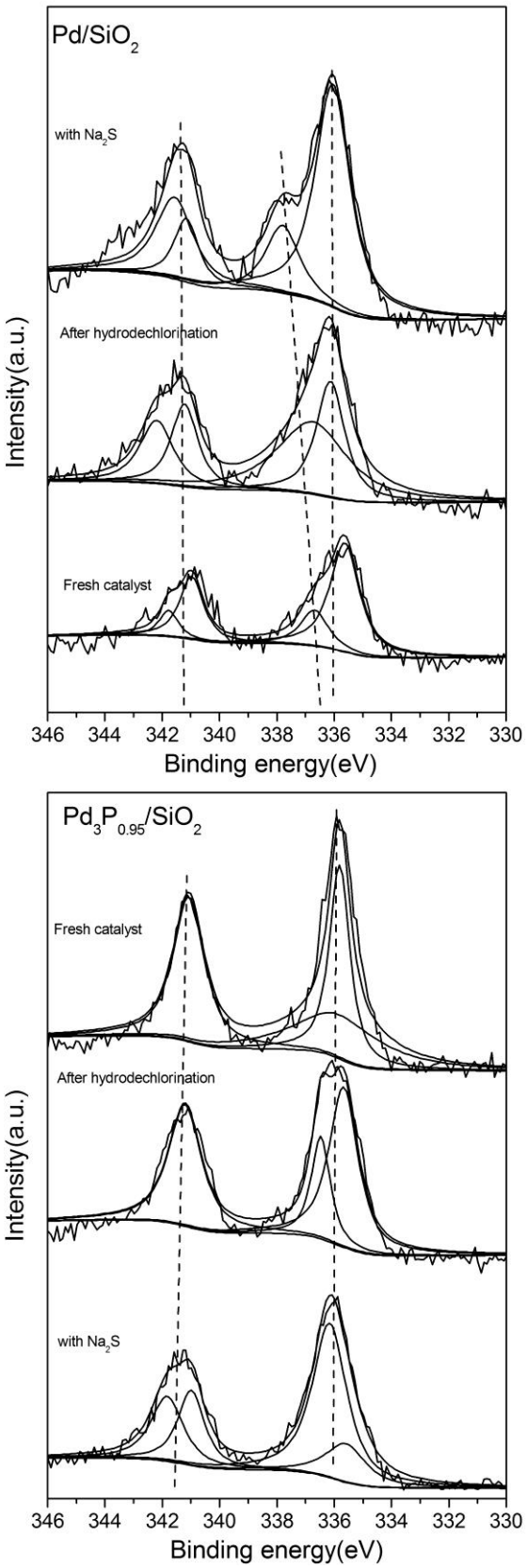

Fig. 3 XPS spectra of the Pd species on SiO_2-supported Pd and $Pd_3P_{0.95}$ samples with 5 wt. % Pd loading.

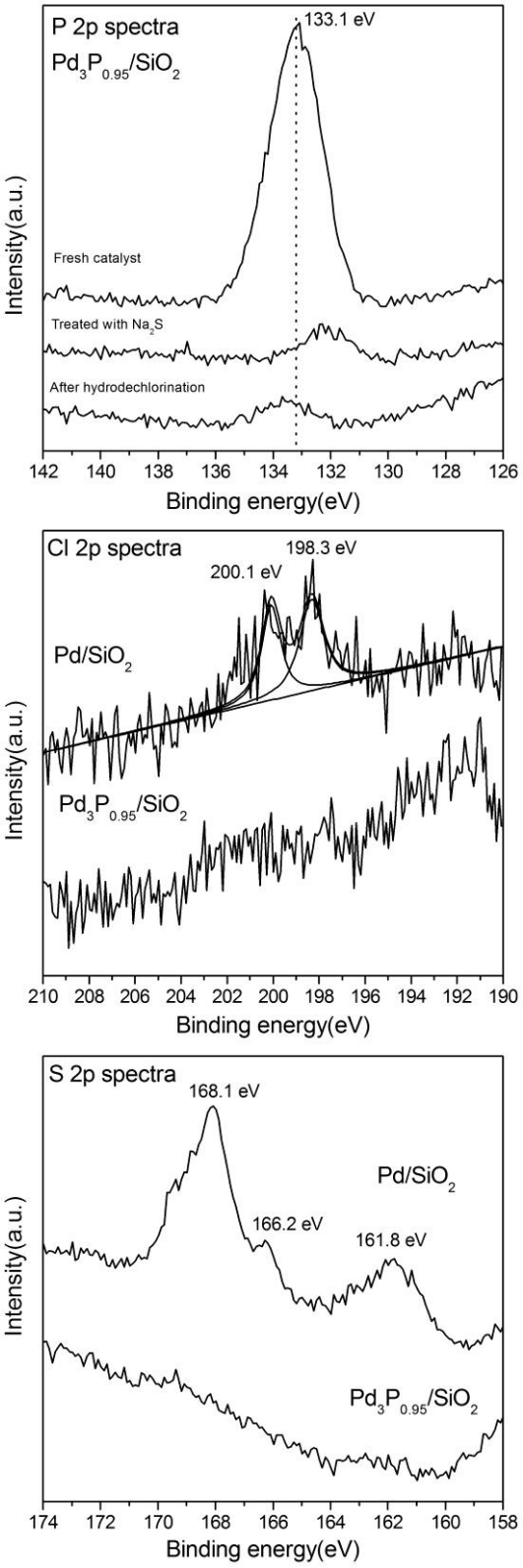

Fig. 4 XPS spectra of P, Cl and S species on SiO_2-supported Pd and $Pd_3P_{0.95}$ samples with 5 wt. % Pd loading.

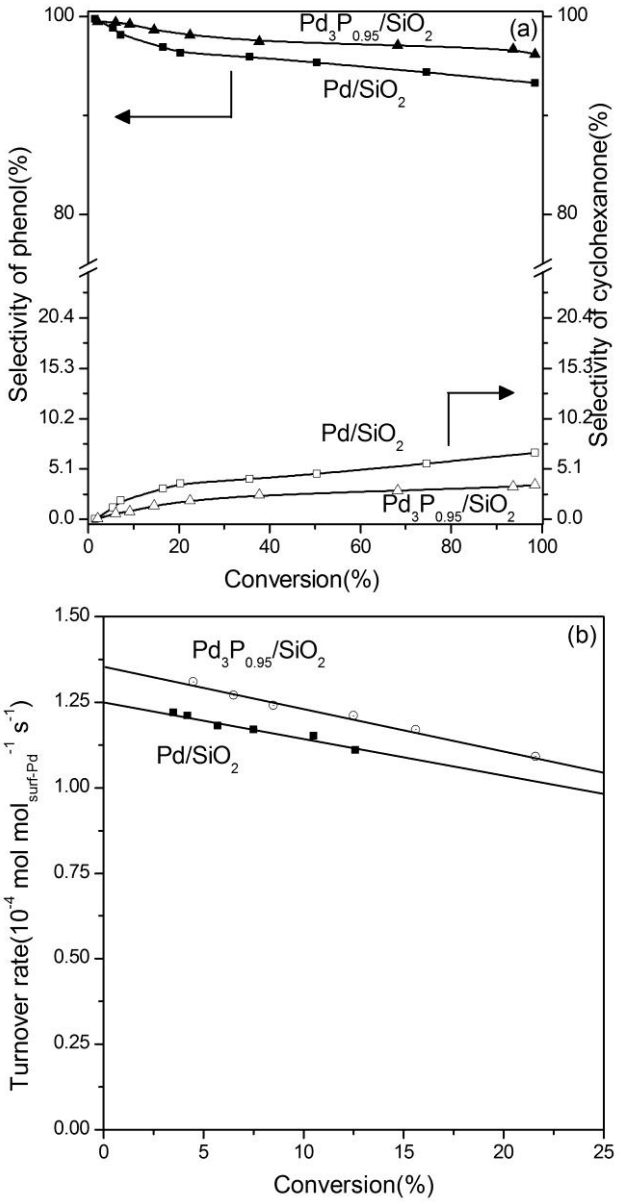

Fig. 5 (a) Product distribution of the 4-CP HDC reaction over the palladium and palladium phosphide catalysts and (b) the effect of the reaction conversion rate on the turnover rate (TOR) of the HDC reaction over the palladium and palladium phosphide catalysts (Initial TOR value, extrapolated to zero conversion (298 K, 3.1 mmol L^{-1} 4-CP)).

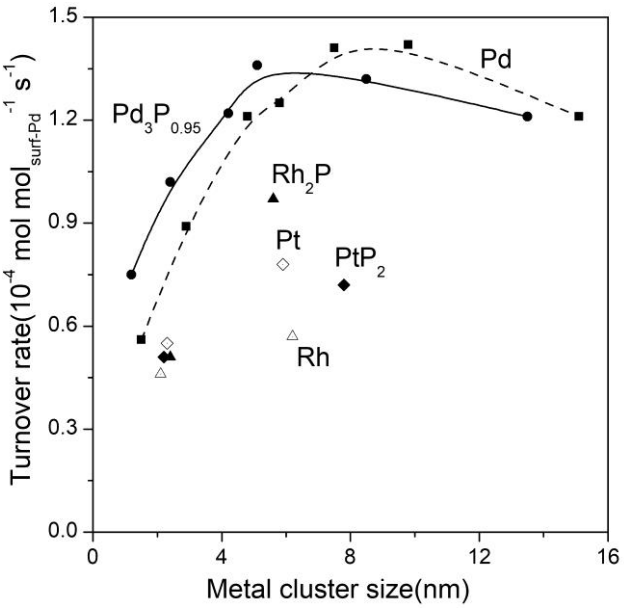

Fig. 6 Effect of the metal and phosphide catalyst cluster size on the initial TOR value for the 4-CP HDC reaction (298 K, 3.1 mmol L^{-1} 4-CP).

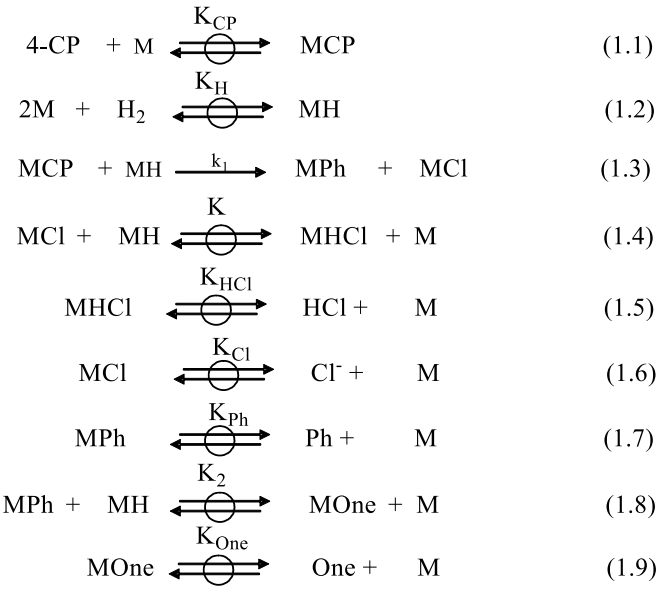

Fig. 7 Proposed reaction pathways for the 4-CP HDC Pd-based catalysts (M is a metal surface site, ⇌ denotes a quasi-equilibrated step, and k_x and K_x are the kinetic and equilibrium constants, respectively, for the individual elementary steps; 4-CP is 4-chlorophenol, Ph is phenol, and one is cyclohexanone.)

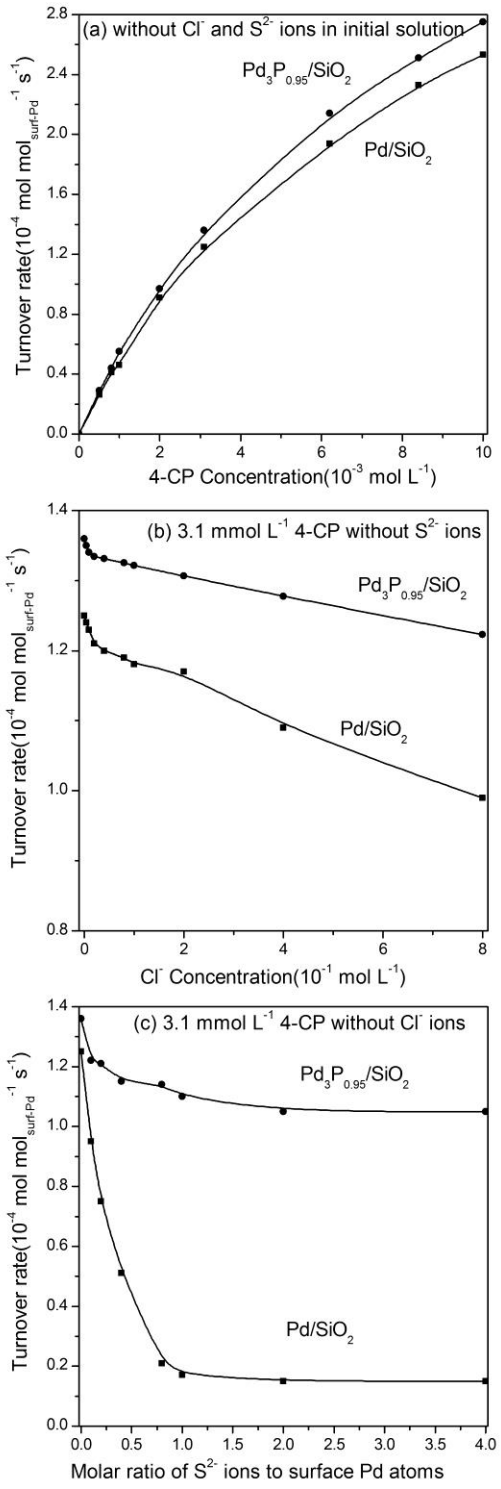

Fig. 8 Influence of (a) the initial 4-CP concentration, (b) the initial Cl^- ion concentration and (c) the initial S^{2-} ion concentration on the initial TOR of the HDC reaction (298 K, 3.1 mmol L^{-1} 4-CP, Pd-based catalysts with 5 wt.% metal loading as shown in entries 4 and 11 in Table 1).

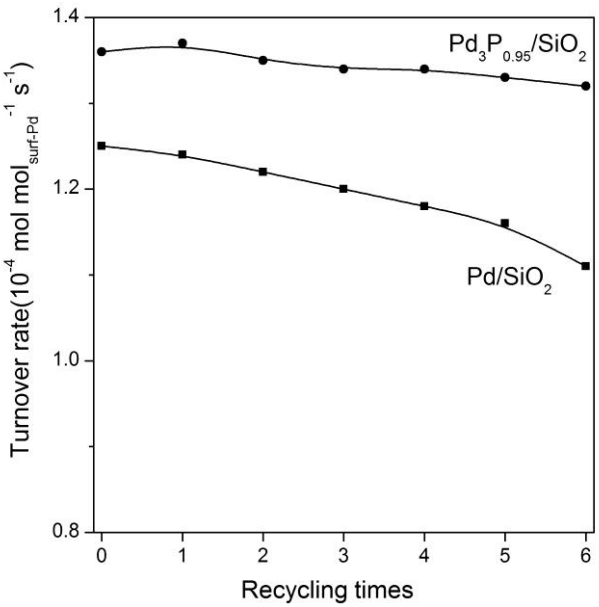

Fig. 9 The initial TOR value of the HDC reaction of 4-CP over Pd-based catalysts with 5 wt.% metal loading (entry 4 an 11 shown in Table 1) during the recycle runs.

Table 1 Metal loading, dispersion, and initial HDC turnover rates of SiO_2-supported metal and metal phosphide catalysts.

Samples	Metal loading (wt. %)		H_2 chemisorptions of metal		Initial HDC turnover rate
	Theoretical	Actual[a]	Dispersion	Particle size (nm)[b]	(10^{-4} mol $mol_{surf\text{-}metal}^{-1}$ s^{-1})[c]
Pd/SiO_2	1	1.1	0.74	1.5	0.56
	2	1.9	0.38	2.9	0.89
	3	1.9	0.23	4.8	1.21
	5	5.1	0.19	5.8	1.25
	5	5.1	0.15	7.5	1.41
	5	5.1	0.11	9.8	1.42
	5	5.1	0.07	15.1	1.21
$Pd_3P_{0.95}/SiO_2$	1	0.9	0.96	1.1	0.75
	2	2.1	0.46	2.4	1.02
	3	2.9	0.26	4.2	1.22
	5	4.9	0.21	5.3	1.36
	7	7.2	0.13	8.5	1.32
	10	10.2	0.08	13.5	1.21
Rh/SiO_2	3	3.0	0.52	2.1	0.46
	5	5.1	0.18	6.2	0.57
Rh_2P/SiO_2	3	2.9	0.45	2.4	0.51
	5	5.1	0.19	5.6	0.97
Pt/SiO_2	3	3.1	0.49	2.3	0.55
	5	5.0	0.18	5.9	0.78
PtP_2/SiO_2	3	2.8	0.50	2.2	0.51
	5	5.3	0.13	7.8	0.72

[a] As determined by ICP.

[b] Mean cluster diameter estimated from the metal dispersion.

[c] (mol of 4-CP)/(mol of surface metal per second), extrapolate to zero conversion (298 K, 3.1 mmol L^{-1} 4-CP).

Table 2 Binding energy of Pd, P, S and Cl species based on XPS data for palladium catalysts with 5 wt.% Pd loading before and after reaction

Sample	Palladium species	Binding energy (eV)						
		Pd $3d_{5/2}$	Pd $3d_{3/2}$	P $2p_{1/2}$	Cl $2p_{1/2}$	Cl $2p_{3/2}$	S $2p_{1/2}$	S $2p_{3/2}$
Pd/SiO_2	Pd^0	335.7	341.0	-	--	--	---	--
$Pd_3P_{0.95}/SiO_2$	Pd^0	335.9	341.2	133.1 (P^{5+})	--	--	--	--
Pd/SiO_2 after HDC reaction	Pd^0	336.2	341.4	--	200.1 (Cl^-)	198.3(Cl-)	--	--
$Pd_3P_{0.95}/SiO_2$ after HDC reaction	Pd^0	335.7	341.1	131.1(P^0)	--	--	--	--
Pd/SiO_2 with Na_2S	Pd^0	336.1	341.4	--	--	--	161.8 (S^{2-})	166.2 (S^{2-})
	Pd^{2+}	337.1	--	--	--	--		168.1 (S^{+6})
$Pd_3P_{0.95}/SiO_2$ with Na_2S	Pd^0	335.8	341.1	133.8 (P^{5+})	--	--		

Table 3 Surface compositions of Pd, P, S and Cl species based on XPS data for palladium catalysts with 5 wt.% Pd loading before and after reaction

Sample	Atomic ratio ($\times 10^{-2}$)			
	P/O	Pd/O	Cl/O	S/O
Pd/SiO_2	--	0.69	--	--
$Pd_3P_{0.95}/SiO_2$	7.01	0.59	--	--
Pd/SiO_2 after HDC reaction	--	0.56	0.99	--
$Pd_3P_{0.95}/SiO_2$ after HDC reaction	0.21	0.67	0	0
Pd/SiO_2 with Na2S	--	0.77	--	5.01
$Pd_3P_{0.95}/SiO_2$ with Na2S	0.28	0.75	--	0

Table 4 Fitting parameters of the L-H model for HDC of 4-CP at pH = 7 with 25 mg of 5 wt. % Pd catalyst loading.

Samples	k (10^{-4} mol $mol_{surf\text{-}Pd}^{-1}$ s^{-1})	K_{CP} (10^{-4} L mol^{-1})	K_{Cl} (10^{-4} L mol^{-1})	R^2
Pd/SiO_2	4.4±0.09	0.15±0.02	0.04±0.002	0.991
$Pd_3P_{0.95}/SiO_2$	4.7±0.15	0.16±0.02	0.01±0.001	0.987